Fermilab

FERMILAB-PUB-08-120-E

Compatibility of high-Δm^2 ν_e and $\bar{\nu}_e$ neutrino oscillation searches

A. A. Aguilar-Arevalo[5], C. E. Anderson[16], A. O. Bazarko[12], S. J. Brice[7], B. C. Brown[7], L. Bugel[5], J. Cao[11], L. Coney[5], J. M. Conrad[5], D. C. Cox[8], A. Curioni[16], Z. Djurcic[5], D. A. Finley[7], B. T. Fleming[16], R. Ford[7], F. G. Garcia[7], G. T. Garvey[9], C. Green[7,9], J. A. Green[8,9], T. L. Hart[4], E. Hawker[3,9], R. Imlay[10], R. A. Johnson[3], G. Karagiori[5], P. Kasper[7], T. Katori[8], T. Kobilarcik[7], I. Kourbanis[7], S. Koutsoliotas[2], E. M. Laird[12], S. K. Linden[16], J. M. Link[14], Y. Liu[11], Y. Liu[1], W. C. Louis[9], K. B. M. Mahn[5], W. Marsh[7], P. S. Martin[7], G. McGregor[9], W. Metcalf[10], P. D. Meyers[12], F. Mills[7], G. B. Mills[9], J. Monroe[5], C. D. Moore[7], R. H. Nelson[4], V. T. Nguyen[5], P. Nienaber[13], S. Ouedraogo[10], R. B. Patterson[12], D. Perevalov[1], C. C. Polly[8], E. Prebys[7], J. L. Raaf[3], H. Ray[9,15], B. P. Roe[11], A. D. Russell[7], V. Sandberg[9], R. Schirato[9], D. Schmitz[5], M. H. Shaevitz[5], F. C. Shoemaker[12], D. Smith[6], M. Soderberg[16], M. Sorel[5], P. Spentzouris[7], I. Stancu[1], R. J. Stefanski[7], M. Sung[10], H. A. Tanaka[12], R. Tayloe[8], M. Tzanov[4], R. Van de Water[9], M. O. Wascko[10], D. H. White[9], M. J. Wilking[4], H. J. Yang[11], G. P. Zeller[5,9], E. D. Zimmerman[4]

(The MiniBooNE Collaboration)

[1] *University of Alabama; Tuscaloosa, AL 35487*
[2] *Bucknell University; Lewisburg, PA 17837*
[3] *University of Cincinnati; Cincinnati, OH 45221*
[4] *University of Colorado; Boulder, CO 80309*
[5] *Columbia University; New York, NY 10027*
[6] *Embry Riddle Aeronautical University; Prescott, AZ 86301*
[7] *Fermi National Accelerator Laboratory; Batavia, IL 60510*
[8] *Indiana University; Bloomington, IN 47405*
[9] *Los Alamos National Laboratory; Los Alamos, NM 87545*
[10] *Louisiana State University; Baton Rouge, LA 70803*
[15] *University of Florida; Gainesville, FL 32611*
[11] *University of Michigan; Ann Arbor, MI 48109*
[12] *Princeton University; Princeton, NJ 08544*
[13] *Saint Mary's University of Minnesota; Winona, MN 55987*
[14] *Virginia Polytechnic Institute & State University; Blacksburg, VA 24061*
[16] *Yale University; New Haven, CT 06520*

(Dated: May 12, 2008)

This article presents the compatibility of experimental data from neutrino oscillation experiments with a high-Δm^2 two-neutrino oscillation hypothesis. Data is provided by the Bugey, Karlsruhe Rutherford Medium Energy Neutrino Experiment 2 (KARMEN2), Los Alamos Liquid Scintillator Neutrino Detector (LSND), and MiniBooNE experiments. The LSND, KARMEN2, and MiniBooNE results are 25.36% compatible within a two-neutrino oscillation hypothesis. However, the point of maximal compatibility is found in a region that is excluded by the Bugey data. A joint analysis of all four experiments, performed in the $\sin^2 2\theta$ vs Δm^2 region common to all data, finds a maximal compatibility of 3.94%. This result does not account for additions to the neutrino oscillation model from sources such as CP violation or sterile neutrinos.

INTRODUCTION

Neutrino oscillations have been reported at three different Δm^2 scales : solar, atmospheric, and high-Δm^2. The solar [1] and atmospheric [2] best-fit results have been observed by several independent experiments, using various neutrino sources and techniques. The high-Δm^2 result, from the LSND detector [3], has yet to be reproduced.

The LSND experiment observed a significant excess of events which are best fit by $\bar{\nu}_\mu \rightarrow \bar{\nu}_e$ oscillations at the $\Delta m^2 \sim 1$ eV^2 scale. The solar and atmospheric best-fit results are at $\Delta m^2 \sim 8^{+0.6}_{-0.4} \times 10^{-5}$ eV^2 and $\Delta m^2 \sim 2.4^{+0.6}_{-0.5} \times 10^{-3}$ eV^2, respectively. This wide spread of Δm^2 scales cannot be accommodated by the three neutrino mass states of the Standard Model. The LSND result is uniquely incompatible with other oscillation observations, and if verified would demand extensions to the Standard Model in the neutrino sector [4] [5].

Prior to 2007, two experiments, KARMEN2 and Bugey, performed searches for oscillations in the region of oscillation parameter space probed by LSND. KARMEN2 [6] conducted an accelerator-based $\bar{\nu}_\mu \rightarrow \bar{\nu}_e$ appearance search. The Bugey [7] reactor experiment probed for oscillations using $\bar{\nu}_e$ disappearance. Neither experiment found evidence for neutrino oscillations. However, a joint analysis [8] between LSND and KARMEN2 found both were compatible with a two-neutrino oscillation hypothesis at 64% confidence level (CL), for

$\Delta m^2 > 0.2$ eV^2, in a region not covered by Bugey.

The MiniBooNE experiment, located at Fermi National Accelerator Laboratory, was designed to fully explore the LSND result. In 2007, MiniBooNE published results from a $\nu_\mu \to \nu_e$ appearance oscillation search [9]. MiniBooNE observed no significant excess of events in an energy range from 475 MeV to 3 GeV. MiniBooNE is presently collecting anti-neutrino data, for use in an $\bar{\nu}_\mu \to \bar{\nu}_e$ appearance oscillation search.

This analysis presents results from the combination of LSND, MiniBooNE, KARMEN2, and Bugey. It is motivated by a need to determine if the LSND excess may be the result of two-neutrino oscillations, in light of these three null experiments. Results presented in this article make use of the MiniBooNE neutrino data set, and do not include the unpublished anti-neutrino data. The compatibility found in this analysis is valid within the framework of standard 2-neutrino oscillations.

INPUT DATA

Data from each experiment are provided in a two-dimensional (2-D) grid of $\sin^2 2\theta$ vs Δm^2. The value at each grid point represents the agreement between the observed data and a 2-neutrino oscillation hypothesis, with signal appropriate to the oscillation parameters at that point. The data sets come in several different formats (log-Likelihood (ln(L)), Δln(L), χ^2), spanning different $\sin^2 2\theta$ vs Δm^2 ranges. An optimal compatibility calculation would make use of the absolute χ^2, as opposed to the $\Delta\chi^2$, which is the change in χ^2 between each grid point and the experiments best fit point. However, we were unable to obtain the absolute χ^2 information from all input experiments. Therefore, our compatibility calculation can only make use of relative $\Delta\chi^2$ information. All input data is transformed into a $\Delta\chi^2$ surface in $\sin^2 2\theta$ vs Δm^2 space, with common $\sin^2 2\theta$ vs Δm^2 binning.

The transformation from the input ln(L), Δln(L) grid to a $\Delta\chi^2$ grid is derived as follows. In the technique of maximum likelihood fitting, a per-event probability $p(x_i|\alpha)$ is constructed, where x_i are the event-measured quantities and α are the theoretical parameters. The goal is to maximize the likelihood, $\mathcal{L}(\alpha)$, the probability of all events in the sample, assuming the given model probability $p(x_i|\alpha)$ for each event,

$$\mathcal{L}(\alpha) = \Pi_i \; p(x_i|\alpha). \tag{1}$$

The technique of χ^2 fitting is a special case of likelihood fitting in which the per event probability is a Gaussian distribution,

$$p(x_i|\alpha) = \frac{1}{\sqrt{2\pi}\sigma_i} \; e^{-\frac{(x_i - f(x_i|\alpha))^2}{2\sigma_i^2}}. \tag{2}$$

Using this per-event probability in a likelihood fit, the log likelihood becomes

$$-\ln \mathcal{L}(\alpha) = \sum_i \frac{(x_i - f(x_i|\alpha))^2}{2\sigma_i^2} + \sum_i \ln \sqrt{2\pi}\sigma_i. \tag{3}$$

The second sum in the $\ln \mathcal{L}$ equation does not typically depend on the theory parameters α. Equation 3 is minimized by minimizing the familiar χ^2 function,

$$\chi^2(\alpha) = \sum_i \frac{(x_i - f(x_i|\alpha))^2}{\sigma_i^2}. \tag{4}$$

From the point of view of minimization, contours, and interpretation of results, there is an equivalence between the likelihood and the χ^2 functions, given by

$$-2 \ln \mathcal{L}(\alpha) = \chi^2(\alpha). \tag{5}$$

To convert between the input ln(L) or Δln(L) data and the χ^2 or $\Delta\chi^2$ used in this analysis, the input data is multiplied by a factor of -2. The validity of this conversion technique has been verified by comparing calculated allowed regions found using the Δln(L) and $\Delta\chi^2$ grids, for LSND and KARMEN2, with those published by these experiments.

The input experiments published observation and limit curves using two different methods. The first method is a two-dimensional (2-D) global scan that calculates the $\Delta\chi^2$ or Δln(L) with respect to the global best fit point across the entire grid. LSND and KARMEN2 calculated their results using this method. The second method is a one-dimensional (1-D) raster scan that calculates the change with respect to the local best fit point in each Δm^2 row. The Bugey and MiniBooNE experiments used this method to produce their exclusion curves. Given the mixture of methods used to report results from the input data, we have performed our compatibility calculation using both methods. For each input experiment we create two $\Delta\chi^2$ grids - one using the 2-D global scan method, and one using the 1-D raster scan method.

The LSND data are provided as a 2-D histogram of ln(L) values containing the decay-in-flight and the decay-at-rest results. The input grid covers 0.000313 to 1.01 in $\sin^2 2\theta$ and 0.0098 to 101.16 eV^2 in Δm^2. The LSND ln(L) grid is first converted into a Δln(L) grid, and then multiplied by -2 to produce a $\Delta\chi^2$ grid. The conversions from ln(L) to Δln(L) and Δln(L) to $\Delta\chi^2$ are tested by calculating the 2-D 90% and 99% CL allowed regions by stepping away from the global best fit point a certain number of units in Δln(L), $\Delta\chi^2$ space. Δln(L) units are 2.3 (90% CL) and 4.6 (99% CL); $\Delta\chi^2$ units are, for a

2-D, 2 degree of freedom scan : 4.61 (90% CL) and 9.21 (99% CL). Both tests properly reproduce the published LSND result [3].

The data from the KARMEN2 experiment are $\Delta\ln(\mathrm{L})$ values covering a range of 0.000316 to 1 ($\sin^2 2\theta$) and 0.01 to 100 eV^2 (Δm^2). Each point is multiplied by -2 to produce a $\Delta\chi^2$ grid. A cross-check is performed using the $\Delta\chi^2$ grid, where the probability is calculated at each point on the grid using 2 degrees of freedom (DOF). Points where the probability crosses 10% delineate the 90% exclusion band. This test correctly finds the 90% CL exclusion band from the KARMEN2 publication [6].

We were unable to obtain data directly from the Bugey collaboration. However, a recent global analysis of Gallium and reactor ν_e disappearance data describes a method used to reproduce the χ^2 surface of Bugey, complete with full systematic errors [10]. The authors kindly provided us with their full χ^2 surface ($\sin^2 2\theta$: 0.01 to 1, Δm^2 : 0.01 to 100 eV^2). A cross-check was also performed on this data by applying the raster scan method and stepping away from each local best fit point by 2.71 $\Delta\chi^2$ units to find the 90% CL exclusion band. Using this method we are able to reproduce the published Bugey result [7].

The MiniBooNE data is expressed as a χ^2 format from 0.0001 to 0.4108 in $\sin^2 2\theta$ and 0.0488 to 51.13 eV^2 in Δm^2. This analysis utilizes the MiniBooNE data from 475 MeV to 3 GeV in neutrino energy; the low energy region (below 475 MeV) is not considered in the compatibility calculation.

COMPATIBILITY CALCULATION

The compatibility calculation uses a method developed by Maltoni and Schwetz [11] to answer the specific question, *"How probable is it that all experimental results come from the same underlying two-neutrino oscillation hypothesis?"*. First, a $\Delta\chi^2$ grid is constructed for each experiment as described in the previous section. The individual grids are then summed together to produce one summed $\Delta\chi^2$ grid. The compatibility test statistic, $\bar{\chi}^2_{min}$, is the minimum of the summed $\Delta\chi^2$ grid. $\bar{\chi}^2_{min}$ follows a χ^2 distribution with P_c degrees of freedom, where P_c is the sum of the total number of independent parameters minus the number of independent parameters estimated from the data. For example, the combination of the 2-D MiniBooNE and 2-D LSND results yields 4 total independent parameters; each experiment independently measures $\sin^2 2\theta$ and Δm^2. Two parameters are estimated from the data ($\sin^2 2\theta$,Δm^2), resulting in a P_c of 2. The final compatibility is the χ^2 probability of $\bar{\chi}^2_{min}$ using P_c degrees of freedom. In the analysis using two experiments P_c is 2, for three experiments P_c is 4, and for all four experiments P_c is 6.

This method is designed to be robust against cases where the χ^2 minima of the individual data sets are very low, and when several parameters are fitted to a large number of data points. It reduces the problem that a possible disagreement between data sets becomes diluted by data points which are insensitive to the crucial parameters.

Of course, there are limitations to this method. This method does not take into account the absolute goodness of fit of each individual experiment at its own best fit point. It is also valid only for truly statistically independent data sets. Theoretical uncertainties in similar experiments may introduce correlations between the various results; for example, LSND and KARMEN2 have the same neutrino beam energy spectrum which may result in similar neutrino interaction errors. However, a previously reported combined analysis of LSND and KARMEN claims the two experiments may be considered independent [8]. MiniBooNE and Bugey are not expected to have any uncertainties in common with the other experiments.

ALLOWED REGION CALCULATION

Combinations of experiments which result in a compatibility of greater than 10% are further explored to locate any remaining allowed regions. Allowed regions are indicated by closed contours in the $\sin^2 2\theta$ vs Δm^2 plane. Contours which do not close form exclusion bands; parameter values situated to the right of the bands are excluded at a given CL (typically 90 and 99% CL). *The allowed regions indicate where the oscillation parameters would lie, at a given confidence level, assuming all experimental results can arise in a framework of two-neutrino oscillations. The calculated compatibility is the metric for how valid this assumption is.*

The allowed regions calculation follows the prescription of Roe [12]. Each experiments $\Delta\chi^2$ grid is converted into a $\Delta\chi^2$ probability grid, using an appropriate number of DOF (2 for the global scan analysis, 1 for the raster scan analysis). The final combined probability at a given point can be obtained from the product of the individual probabilities, x. The result is a sum of powers of the absolute value of the logarithms of x,

$$Prob = x \cdot \sum_{j=0}^{n-1} \frac{1}{j!} \cdot |ln^j(x)| \qquad (6)$$

, where x is the product of the individual probabilities and n is the number of experiments being included. Points where the probability crosses 10% bound the 90% confidence level allowed region; points where the probability crosses 1% bound the 99% region.

There has been much discussion regarding the number of degrees of freedom (DOF) that one can use with the

χ^2 grids in the allowed region calculation, and how the DOF changes across the grids [13]. We examined the change in DOF across the 2-D grid, using the Feldman-Cousins frequentist method [13]. Our study of the DOF finds that, in general, use of 2 DOF is valid across the 2-D grid. This breaks down for points with high Δm^2 and high $\sin^2 2\theta$ values : $\Delta m^2 > 10$ eV^2 and $\sin^2 2\theta > 0.01$. However, the approximation of 2 DOF is still valid for $\sin^2 2\theta > 0.01$ and $\Delta m^2 < 10$ eV^2. The region where the 2 DOF approximation is no longer valid is an area which does not contain any allowed regions from LSND, and as such should not impact this analysis.

The compatibility is defined as the $\Delta\chi^2$ probability at the best fit point. The combination of experiments reduces the number of independent parameters used in the probability calculation. The Maltoni-Schwetz method can easily accommodate the change in degrees of freedom [11]. It is not clear how to include information about the number of degrees of freedom into the more traditional (Roe) method (Equation 6). The Roe method applied as-is results in too high a compatibility, due to the inability of the method to consider a reduced degree of freedom.

We have chosen to use the more traditional Roe method to calculate the allowed regions, and the Maltoni-Schwetz method to find the compatibility. Equivalently, we could have chosen to use the generic Maltoni-Schwetz method to find the allowed regions; both methods return identical values when evaluating the joint probability distribution function (PDF).

The range of $\sin^2 2\theta$ vs Δm^2 common to all experiments is used for the compatibility and allowed region calculations. The Δm^2 is restricted to 0.0488 to 51.13 eV^2 for all results. The $\sin^2 2\theta$ range, for results without Bugey, is 0.000317 to 0.4108. Results containing Bugey employ a $\sin^2 2\theta$ range of 0.01 to 0.4108.

HOW TO INTERPRET THE RESULTS

As previously discussed, the $\Delta\chi^2$ grids used in this analysis are created in two ways. The 2-D grids use the global best fit point internal to each experiment to produce the $\Delta\chi^2$. The compatibility extracted from the combined 2-D $\Delta\chi^2$ grid represents how probable it is that one could observe the experimental results if nature truly has two neutrino oscillations in this high-Δm^2 region (0.0488 to 51.13 eV^2). This method also finds the most probable point for the true oscillations to exist across the evaluated phase space. The 1-D results use a raster scan method to find the local best fit point at each Δm^2, internal to each experiment, to produce the $\Delta\chi^2$. The results from this method represent the compatibility at each Δm^2, if nature truly had two neutrino oscillations located at that Δm^2.

RESULTS

The 2-D analysis reports a single value for the maximum compatibility of the experimental data with the two neutrino oscillation hypothesis. These results are presented in Table I. The compatibility for the 1-D analysis is a function of Δm^2, and is presented in graphical form in the following sections. All results are calculated with respect to an oscillation hypothesis valid in the Δm^2 region of 0.0488 to 51.13 eV^2. This region has been further divided into three components ; low Δm^2 indicates the region from 0.0488 to $\sim$1 eV^2, medium Δm^2 spans $\sim$1 to $\sim$7 eV^2, and high Δm^2 is $>\sim$7 eV^2. These divisions are used to characterize the results in the following sections.

We first present results from the combination of the three accelerator-based appearance oscillation experiments (LSND, KARMEN2, MiniBooNE). This combination finds a high compatibility (25.36%) at low Δm^2 (Figure 1). The inclusion of the Bugey reactor disappearance data highly constrains the low Δm^2 region, reducing the compatibility to a low level (3.94%, Figure 4). In the second section, the compatibility and allowed regions are explored in various combinations of the null experiments (KARMEN2, MiniBooNE, and Bugey). In the third section, the result of 2.14% compatibility omits the KARMEN2 data. The final section discusses the combination of LSND and KARMEN2.

LSND	KARMEN2	MB	Bugey	Max Compat (%)	Δm^2	$\sin^2 2\theta$
X	X	X		25.36	0.072	0.256
X	X	X	X	3.94	0.242	0.023
	X	X		73.44	0.052	0.147
	X	X	X	27.37	0.221	0.012
X		X		16.00	0.072	0.256
X		X	X	2.14	0.253	0.023
X	X			32.21	0.066	0.4

TABLE I: Maximum compatibility for a variety of combinations of the input experiments, found using the 2-D $\Delta\chi^2$ grids. The last two columns indicate the Δm^2 vs $\sin^2 2\theta$ location of the point of maximum compatibility. The X's indicate which experiments were included in the analysis.

LSND, KARMEN2, MiniBooNE

First, we consider only results from the ν_e appearance searches. Figure 1 (top) displays the 2-D $\Delta\chi^2$ grid from the combination of LSND, KARMEN2, and MiniBooNE. The point of maximal compatibility (25.36%) is indicated by the star. The point of highest compatibility is not limited by the $\sin^2 2\theta$ vs Δm^2 grid boundaries, but is found in a region excluded by the Bugey data. The allowed re-

gions for two-neutrino oscillations are shown in the bottom of Figure 1. There are 99% allowed regions at low, medium, and high Δm^2. The only 90% allowed region is located at low Δm^2, which overlaps slightly with the LSND 90% allowed region.

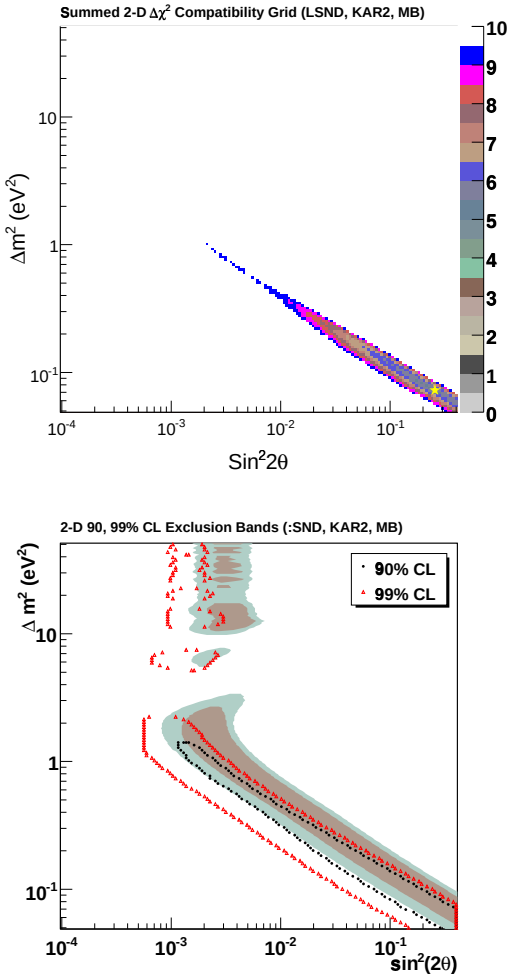

FIG. 1: Top : Summed 2-D $\Delta\chi^2$ compatibility grid from LSND, KARMEN2, and MiniBooNE. The star indicates the point of maximal compatibility (25.36%). Bottom : Allowed regions (90%, 99%) found for the 2-D LSND, KARMEN2, and MiniBooNE joint analysis. Red points contain the 99% CL region, black points contain the 90% CL region. The solid brown area is the LSND 90% allowed region; the solid light blue area is the LSND 99% allowed region. The vertical straight edge on the left arises from a sharp discontinuity in the LSND input grid.

Compatibility values are also reported for the 1-D analysis as a function of Δm^2. The maximum compatibility for the 1-D LSND, KARMEN2, MiniBooNE analysis is shown in the top of Figure 2. The 1-D analysis also finds a high compatibility (here almost 50%) at low Δm^2. In addition, this raster scan method allows for a ∼25% compatible region at medium Δm^2. Figure 2 (bottom) illustrates the 90 and 99% allowed regions. While these regions appear to be shifted from the LSND signal region, it must be remembered that the LSND signal region shown is that found using a 2-D analysis, *not* a 1-D scan.

Finally, Figure 3 compares the LSND allowed regions found using the 1-D $\Delta\chi^2$ method to those published by the LSND collaboration, found using the 2-D scan. The 1-D allowed regions are quite large in comparison to the 2-D regions, and include areas which had no 90% allowed islands in the 2-D scan.

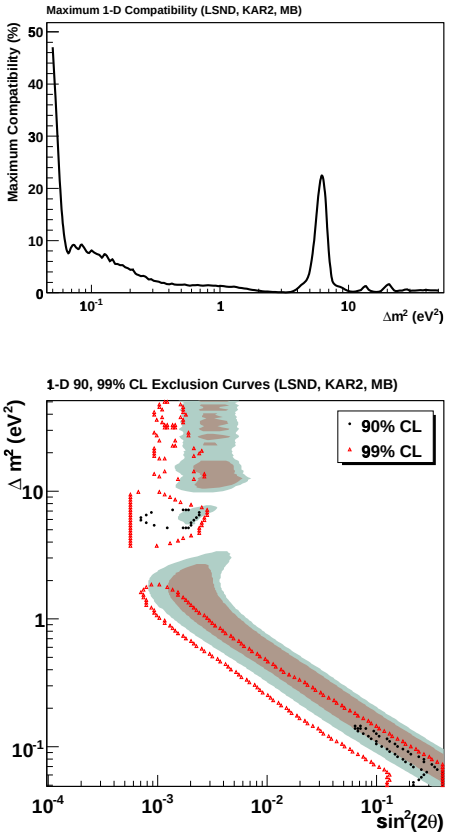

FIG. 2: Top : Maximum compatibility as a function of Δm^2 for the 1-D LSND, KARMEN2, MiniBooNE analysis. Bottom : Allowed regions for the 1-D LSND, KARMEN2, MiniBooNE analysis. 90% allowed regions exist in the low and mid Δm^2 regions. Red points contain the 99% CL region, black points contain the 90% CL region. The vertical straight edge on the left arises from a sharp discontinuity in the LSND input grid.

LSND, KARMEN2, MiniBooNE, Bugey

The inclusion of the Bugey data significantly changes the compatibility results. The Bugey $\sin^2 2\theta$ range has a lower bound at 0.01; analyses including Bugey are restricted to $\sin^2 2\theta$ of 0.01 to 0.4108. The combination of all four experiments has a 2-D compatibility of 3.94%.

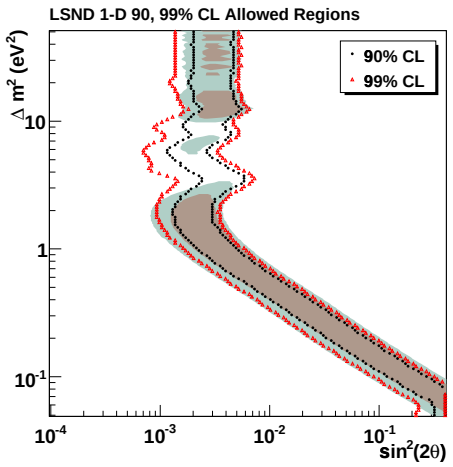

FIG. 3: 90 and 99% allowed regions for the 1-D scan of LSND, overlayed on the 2-D published allowed regions. Red points contain the 99% CL region, black points contain the 90% CL region.

Figure 4 shows the final 2-D $\Delta\chi^2$ grid, for all four experiments.

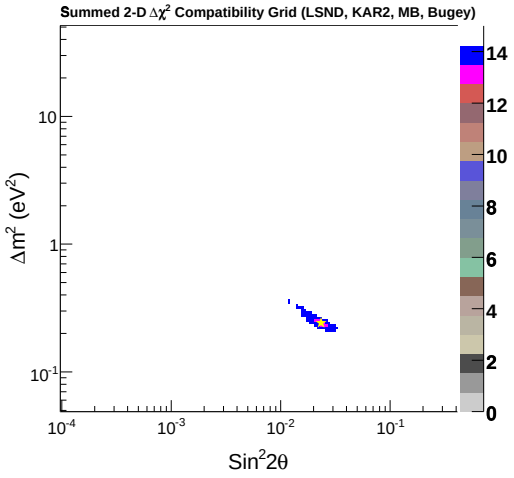

FIG. 4: Summed 2-D $\Delta\chi^2$ compatibility grid from LSND, KARMEN2, MiniBooNE, Bugey. The star indicates the point of maximal compatibility (3.94%).

The 1-D analysis of all four experiments agrees quite well with the 2-D results; the point of highest compatibility is found in the low Δm^2 region, and all results are no more than 5.2% compatible with having resulted from two-neutrino oscillations (Figure 5).

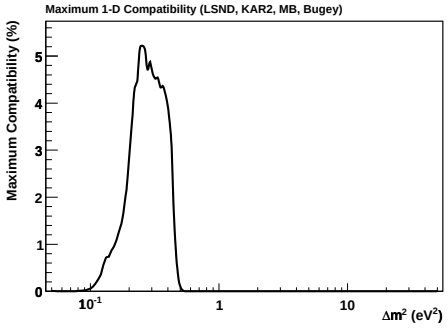

FIG. 5: Maximum compatibility as a function of Δm^2 for the 1-D LSND, KARMEN2, MiniBooNE, Bugey analysis.

KARMEN2, MiniBooNE

It is instructive to calculate compatibility and remaining allowed regions, in the absence of a positive LSND signal. The 2-D analysis finds KARMEN2 and MiniBooNE are 73.44% compatible with a two-neutrino hypothesis; there is a 73.44% chance that we would find these two null results, in the presence of two-neutrino oscillations at these $\sin^2 2\theta$, Δm^2 values (0.147, 0.052 eV^2). However, the minimum in the $\Delta\chi^2$ is outside of the region where either experiment has much sensitivity. For example, the compatibility at the lowest grid point (0.0003, 0.05 eV^2) still remains high at 53.52%. The summed $\Delta\chi^2$ and allowed regions for oscillations are shown in Figure 6.

The 1-D analysis of KARMEN2 and MiniBooNE finds high compatibility that reaches 100% at low and medium Δm^2 (top, Figure 7). However, the 90 and 99% CL exclusion curves (bottom, Figure 7) are almost identical to those found in the 2-D analysis.

KARMEN2, MiniBooNE, Bugey

If we ignore the positive LSND result, but now include Bugey, it is 27.37% probable that we would have found all three null results in a world with two-neutrino ($\Delta m^2 > 0.0488$ eV^2) oscillations. Please note that the point of maximal compatibility is limited by the boundary of the analyzed region. Figure 8 (top) shows the 2-D compatibility of all three null results. Figure 8 (bottom) presents the remaining allowed regions. The straight line on the left hand side is an artifact of the requirement that the analysis be performed over regions of phase space common to all experiments.

The 1-D analysis of KARMEN2, MiniBooNE, and Bugey (top, Figure 9) produces a higher degree of compatibility than the 2-D analysis shown in Table I, but agrees with the remaining allowed regions (bottom, Figure 9).

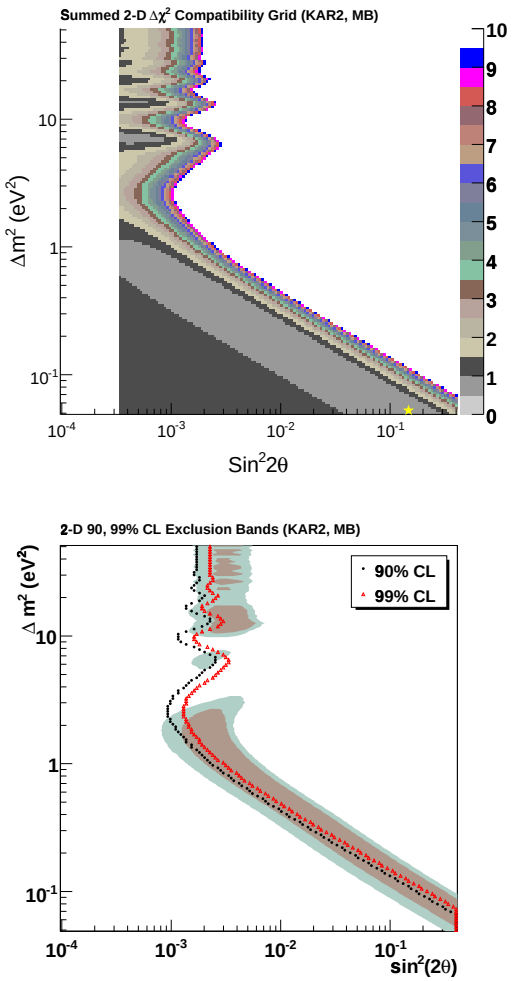

FIG. 6: Top : Summed $\Delta\chi^2$ compatibility of KARMEN2 and MiniBooNE using the 2-D analysis. The star indicates the point of maximal compatibility (73.44%). The compatibility is limited by the boundaries of the analysis and may increase with a loosening of the grid range. Bottom : Exclusion bands (90%, 99%) found for the 2-D KARMEN2 and MiniBooNE joint analysis. Values to the right of the lines are excluded at the 90, 99% CL. Red points form the 99% CL band, black points form the 90% CL band.

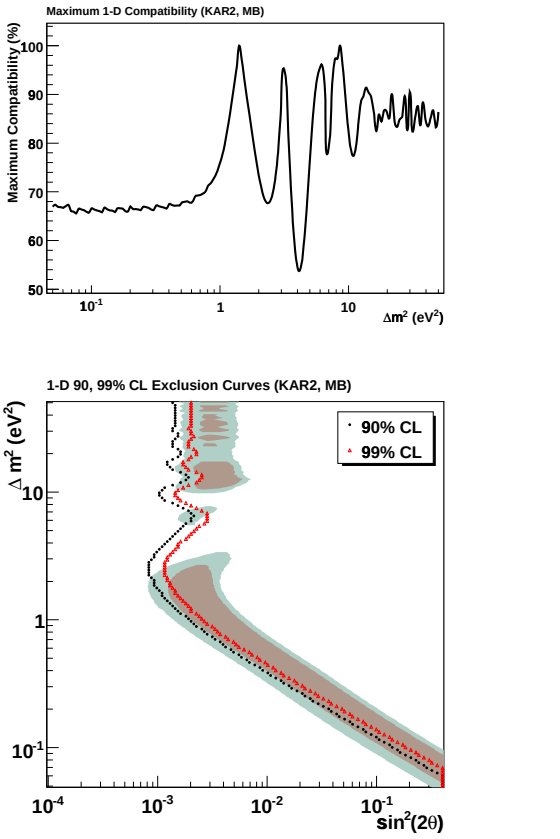

FIG. 7: Top : Maximum compatibility as a function of Δm^2 for the 1-D KARMEN2 and MiniBooNE analysis. Bottom : Exclusion bands (90%, 99%) found for the 1-D KARMEN2, MiniBooNE joint analysis. Values to the right of the lines are excluded at the 90, 99% CL. Red points form the 99% CL band, black points form the 90% CL band. These curves are very similar to those found using the 2-D method in Figure 6.

LSND, MiniBooNE

Table I presents results from the combination of LSND and MiniBooNE, not including the KARMEN2 result. The compatibility from the 2-D analysis is actually lower than that found from the combination of LSND, KARMEN2, and MiniBooNE. KARMEN2 and MiniBooNE are complementary results; KARMEN2 has the most power in high Δm^2 regions, while MiniBooNE is most sensitive to the lower Δm^2 areas. The maximum compatibility of the (LSND, MiniBooNE), and (LSND, KARMEN2, MiniBooNE) analyses is found in the low Δm^2 region where MiniBooNE has the most power. The inclusion of KARMEN2 data adds two degrees of freedom, but very little resolving power in this area of phase space. Figure 10 illustrates this effect by overlaying the 2-D LSND 90 and 99% allowed regions with the MiniBooNE and KARMEN2 2-D 90% exclusion curves.

MiniBooNE previously reported a 2% compatibility for the combination of LSND and MiniBooNE, found using the 1-D raster scan method [9]. The prior result was calculated over a restricted Δm^2 range (0.2 to 0.7 eV^2). The current analysis, when restricted to the same Δm^2 range, agrees with the previously published result.

LSND, KARMEN2

The maximum compatibility of LSND and KARMEN2, found using the 2-D method, is 32.21%. This differs from a previously reported compatibility of 64% [8].

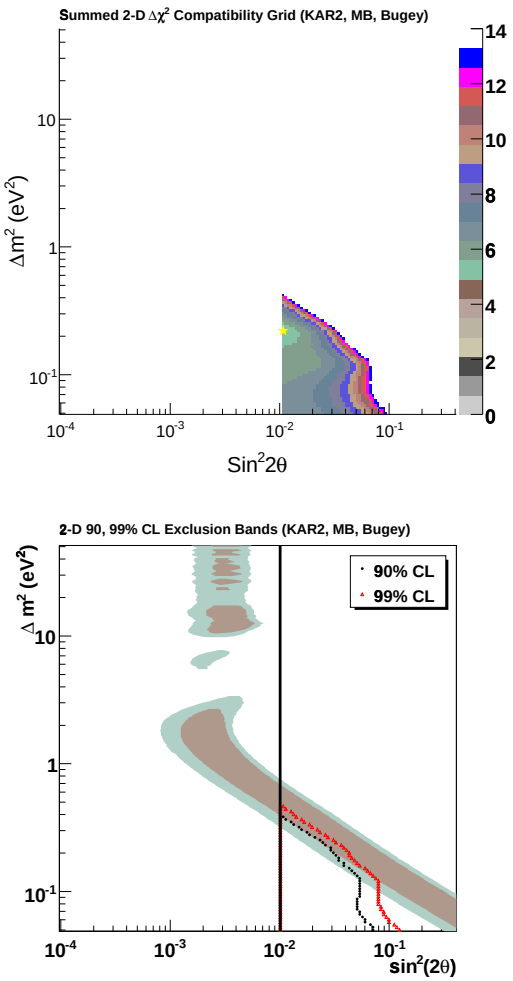

FIG. 8: Top : Summed 2-D $\Delta\chi^2$ compatibility grid from KARMEN2, MiniBooNE, and Bugey. The star indicates the point of maximal compatibility (27.37%). Bottom : Exclusion bands (90%, 99%) found for the 2-D KARMEN2, MiniBooNE, and Bugey joint analysis. Values to the right of the lines are excluded at the 90, 99% CL. Red points form the 99% CL band, black points form the 90% CL band. The vertical straight edge on the left indicates the lower $\sin^2 2\theta$ bound of 0.01.

There are two differences between the current analysis and the study by Church *et al.* : the input LSND data set (this analysis utilizes the LSND decay-in-flight and decay-at-rest results, while the previous analysis only used the LSND decay-at-rest data), and the method used to define and calculate the compatibility. Both analyses find a high compatibility between LSND and KARMEN2.

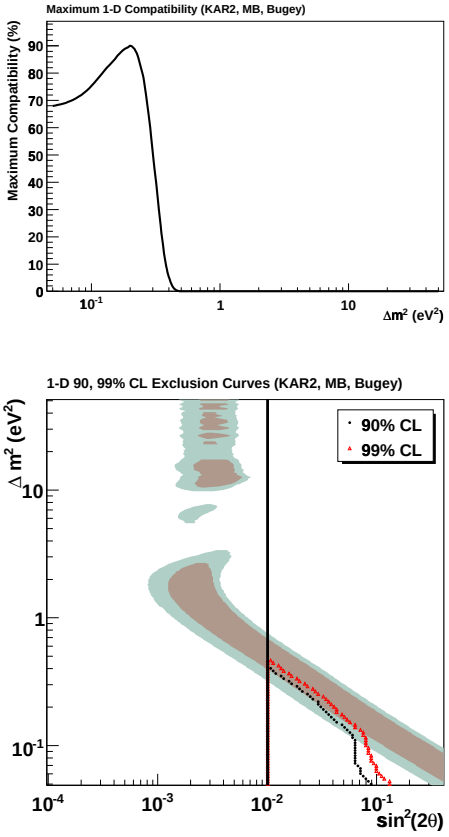

FIG. 9: Top : Maximum compatibility as a function of Δm^2 for the 1-D KARMEN2, MiniBooNE, and Bugey analysis. Bottom : Exclusion bands (90%, 99%) found for the 1-D KARMEN2, MiniBooNE, Bugey joint analysis. Values to the right of the lines are excluded at the 90, 99% CL. Red points form the 99% CL band, black points form the 90% CL band. The vertical straight edge on the left indicates the lower $\sin^2 2\theta$ bound of 0.01.

CONCLUSIONS

We present results on the compatibility of different combinations of four experiments which have searched for neutrino oscillations at the high Δm^2 scale ($>$ 0.0488 eV^2). The LSND experiment has observed a significant excess of events; the other three experiments report null results and set limits on the oscillation parameter space. The compatibility has been calculated using both a 2-D and a 1-D scan technique with the method of Reference [11]. Remaining allowed regions have been found for combinations resulting in greater than 10% compatibility. Results from the 2-D scan indicate that LSND, KARMEN2, and MiniBooNE are 25.36% compatible with having come from two-neutrino oscillations. However, the best fit point for this analysis is found in a region excluded by Bugey. (This point is also excluded by other reactor experiments such as

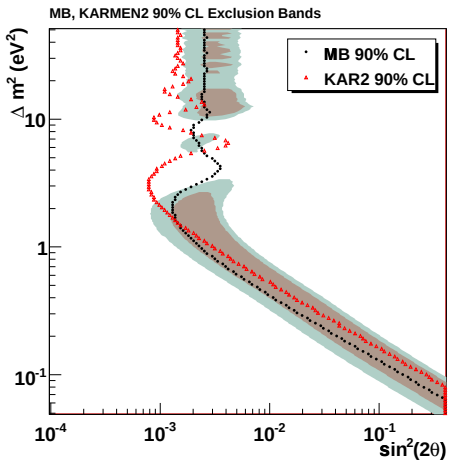

FIG. 10: LSND 90, 99% CL allowed regions, overlayed with the KARMEN2 (red) and MiniBooNE (black) 2-D 90% CL exclusion bands. KARMEN2 is more powerful at excluding high Δm^2 values while MiniBooNE is more powerful in the low Δm^2 region.

Goesgen [14], and Krasnoyarsk [15].) The 2-D scan from all four experiments including Bugey, in a limited $\sin^2 2\theta$ region common to all experiments, finds they are only 3.94% compatible with two-neutrino oscillations. This analysis does not take into consideration the absolute goodness of fit of each individual experiment at its own best fit point, or any additional non-Standard Model effects such as CP violation or sterile neutrinos.

We acknowledge the support of Fermilab, the Department of Energy, and the National Science Foundation. We thank M. Acero, C. Giunti, and M. Laveder for providing us with the Bugey data. We thank K. Eitel for providing us with the KARMEN2 data.

[1] S. Ahmed et al. [SNO Collaboration], Phys. Rev. Lett. 92, 181301 (2004), arXiv:nucl-ex/0309004.
[2] G. Fogli et al., Phys. Rev. D 67, 093006 (2003), arXiv:hep-ph/0303064.
[3] C. Athanassopoulos *et al.*, Phys. Rev. Lett. 75, 2650 (1995); 77, 3082 (1996); 81, 1774 (1998); A. Aguilar *et al.*, Phys. Rev. D 64, 112007 (2001).
[4] M. Sorel, J. Conrad, M. Shaevitz, Phys. Rev. D 70, 073004 (2004).
[5] G. Karagiorgi *et al.*, Phys. Rev. D 75, 013011 (2007).
[6] B. Armbruster *et al.*, Phys. Rev. D 65, 112001 (2002).
[7] B. Achkar *et al.*, Nucl. Phys. B434, 503 (1995).
[8] E. Church *et al.*, Phys. Rev. D 66, 013001 (2002).
[9] A.A. Aguilar-Arevalo *et al.*, Phys. Rev. Lett. 98, 231801 (2007).
[10] M. Acero *et al.*, hep-ph/0711.4222v2 (2007).
[11] M. Maltoni, T. Schwetz, Phys. Rev. D 68, 033020 (2003).
[12] B. Roe, *Probability and Statistics in Experimental Physics* (Springer, New York, 2001), pg 162-164.
[13] G. Feldman, R. Cousins, Phys. Rev. D 57, 3873 (1998).
[14] G. Zacek *et al.*, Phys. Rev. D 34, 2621 (1986).
[15] G.S. Vidyakin *et al.*, JETP Lett. 59, 364 (1994).